Dalton Transactions

Effects of the non-covalent interactions on the electronic and electrochemical properties of Cu(I) biquinoline complexes

Journal:	*Dalton Transactions*
Manuscript ID	DT-ART-07-2018-002722.R1
Article Type:	Paper
Date Submitted by the Author:	14-Aug-2018

Complete List of Authors:	Martínez, Natalia P.; Pontificia Universidad Catolica de Chile, Facultad de Química Isaacs Casanova, Mauricio; Pontificia Universidad Catolica de Chile, Facultad de Química; Centro de Investigación en Nanotecnologia y Materiales Avanzados CIEN-UC; UC-Energy Research Center Oliver, Allen; University of Notre Dame, Department of Chemistry and Biochemistry Ferraudi, Guillermo; University of Notre Dame, Department of Chemistry and Biochemistry; Radiation Laboratory, University of Notre Dame Lappin, Alexander; University of Notre Dame, Department of Chemistry and Biochemistry Guerrero, Juan; Universidad de Santiago de Chile, Facultad de Química y Biología

Dalton Transactions

ARTICLE

Effects of the non-covalent interactions on the electronic and electrochemical properties of Cu(I) biquinoline complexes

Received 00th January 20xx,
Accepted 00th January 20xx

DOI: 10.1039/x0xx00000x

www.rsc.org/

Natalia P. Martínez,[a] Mauricio Isaacs,[a,b,c,] Allen G. Oliver,[d] G. Ferraudi,[d,e] A. Graham Lappin,[d*] Juan Guerrero.[f*]

The Cu(I) complex {[Cu^{I}(*biq*)$_2$]ClO$_4$-*biq*} with *biq* = 2,2-biquinoline, was prepared, fully characterized and its properties compared with those of the well-known [Cu^{I}(*biq*)$_2$]ClO$_4$ complex. The crystal structures were obtained for both complexes (crystal structure for [Cu^{I}(*biq*)$_2$]ClO$_4$ has not been previously reported). Complex [Cu^{I}(*biq*)$_2$]ClO$_4$ crystallizes as a racemate where each enantiomer has a different τ4 value while compound {[Cu^{I}(*biq*)$_2$]ClO$_4$-*biq*} crystallizes as a non-chiral supramolecular aggregate with an uncoordinated *biq* molecule forming a π–π stacking interaction with a coordinated *biq*. The ^{1}H-NMR spectroscopy in non-coordinating solvents reveals that structures in solution are similar to those in the solid phase, confirming the presence of a supramolecular arrangement for compound {[Cu^{I}(*biq*)$_2$]ClO$_4$-*biq*}. Stability of the non-covalent aggregate in solution of {[Cu^{I}(*biq*)$_2$]ClO$_4$-*biq*} causes significant differences between the spectroscopic and electrochemical properties of {[Cu^{I}(*biq*)$_2$]ClO$_4$-*biq*} and [Cu^{I}(*biq*)$_2$]ClO$_4$.

Introduction

Supramolecular motifs formed by aggregates of two or more complex units held together by non-covalent interactions are interesting systems because of their intrinsic chemical and physical properties.[1,2] Various non-covalent interactions of differing energies may result in the reversible production of highly structured molecular architectures, quite different from those possible with conventional covalent bonds.[3–5] In the last few decades there has been a significant increase in publications describing the preparation and properties of supramolecular materials such as catenanes, rotaxanes, knots, helicates, dendrimers, racks, grids, boxes, and macrocycles.[6–13] Most result from self-assembly of molecules that act as building units through self-recognition elements. In metal complexes, these element correspond to particular features of the ligands and metals, which act synergistically as preorganizers of the supramolecular arrangements.[14,15]

Copper(I) complexes have played an important role in the development of supramolecular chemistry.[16] The characteristic lability of copper(I) together with an accommodating tetrahedral symmetry is consistent with the conditions required for the assembly of supramolecular structures.[10,17] Consequently, a large number of copper(I) complexes showing the presence of structural assemblies governed by non-covalent interactions has been documented.[10,17] In complexes with large π system in their ligands, such as 2,2'-biquinoline, the stacking stability in the solid phase is principally provided by π-π interactions.[18–21] It has been proposed that physical and chemical properties of materials based on coordination complexes can be supramolecularly tunable, however most examples refer to effects of non-covalent intramolecular interactions on the properties of the complexes themselves.[20,22,23]

However only a few examples of metal complexes presenting a supramolecular assembly that is sufficiently stable for study in solution have been reported, although such effects in reaction kinetics have been explored.[24] In previous work we have shown that the mixed complex [Cu(N-{4-nitrophenyl}pyridine-2-yl-meth-animine)(PPh$_3$)Br] retains a supramolecular dimeric structure in solution, supported in π-π and Br···H non-covalent interactions, that is similar to the structure observed in the crystalline state.[25] In this study, we report a new {[Cu(*biq*)$_2$]ClO$_4$-*biq*} complex which crystallizes in a supramolecular assembly with one additional, uncoordinated ligand. We have used 1D and 2D NMR techniques to examine the structural behaviour in solution and compared optical and electrochemical properties with those shown by the analogous [Cu(*biq*)$_2$]ClO$_4$ complex. Although complex [Cu(*biq*)$_2$]ClO$_4$ has

[a] *Facultad de Química, Pontificia Universidad Católica de Chile, Vicuña Mackenna 4860, 7820436 Macul, Santiago, Chile.*
[b] *Centro de Investigación en Nanotecnología y Materiales Avanzados CIEN-UC, Pontificia Universidad Católica de Chile, Chile.*
[c] *UC-Energy Research Center, Pontificia Universidad Católica de Chile, Chile.*
[d] *Department of Chemistry & Biochemistry, University of Notre Dame, Notre Dame, IN 46556-5670, USA.*
E-mail: alexander.g.lappin.1@nd.edu
[e] *Radiation Laboratory, University of Notre Dame, Notre Dame, IN 46556-5670, USA.*
[f] *Facultad de Química y Biología, Universidad de Santiago de Chile, Libertador Bernardo O'Higgins 3363, Estación central, Santiago, Chile.*
E-mail: juan.guerrero@usach.cl

Electronic Supplementary Information (ESI) available: For ESI and crystallographic data in CIF, CCDC 1588824-1588825. See DOI: 10.1039/x0xx00000x

been known for more than 50 years, its crystal structure has not been reported, and so we also report the structure determined by single-crystal X-ray diffraction.

Results and discussion

Crystallographic structures: A summary of crystal data and structure refinement for complexes {[Cu^{I}(*biq*)$_2$]ClO$_4$-*biq*} and [Cu(*biq*)$_2$]ClO$_4$ is presented in table S1. The structure of compound {[Cu^{I}(*biq*)$_2$]ClO$_4$-*biq*} reveals that the copper cation, perchlorate anion and free biquinoline molecule all crystallize about symmetry elements (Fig. 1A). This complex is the structural isomorph of the BF_4 salt previously reported by Ali *et al*.[26] however that work was done in solid state without studies in solution. The copper complex and perchlorate crystallize on independent two-fold axes (at [0.75, y, 0.25] and [0.25, y, 0.25], respectively) and the free biquinoline molecule about an inversion center at [0.5, 0.5, 0.5]. The Cu center adopts a four-coordinate, distorted tetrahedral geometry (Table 1 for details, τ_4 = 0.73) and is coordinated by four nitrogen atoms from two *biq* ligands.[27] Bond distances about the Cu center are comparable with those found in related Cu complexes containing polypyridine ligands. The two coordinating *biq* ligands are almost orthogonal to each other (angle formed by the two, five-atom planes: [Cu1-N1-C9-C10-N2-(Cu1)] is 87.28(4)°). As expected, the quinoline moieties in each biquinoline molecule (ligand and free molecule) are essentially co-planar (Table 2). In contrast to the enforced *syn*-geometry of the coordinated *biq* ligand, the quinoline groups of the free *biq* molecule adopt an *anti*-conformation. The free *biq* molecule is located in a space between *biq* ligands of two copper complexes in the lattice (Fig. 1B, green/yellow, copper complexes and light blue free *biq).* The close intermolecular contacts from the free *biq* molecule to the neighbouring coordinated *biq* ligands demonstrate a high degree of π-π stacking with centroid to centroid contacts less than 3.6 Å (Table 3). More critically, the centroid to shortest perpendicular contacts are also short, well within Van der Waals contacts. The motif in the lattice is pairs of Cu cations sandwiching the uncoordinated biquinoline between coordinated biquinoline ligands. There is further π-stacking overlap of the terminal phenyl moiety of each coordinated quinoline ring forming a π-stacked layer with another phenyl moiety on an adjacent cation.

The structure of compound [Cu^{I}(*biq*)$_2$]ClO$_4$ reveals that there are two crystallographically independent cations, associated anions and five water molecules of crystallization within the lattice (Fig. 2A). Similar to compound {[Cu^{I}(*biq*)$_2$]ClO$_4$-*biq*}, the copper centers in compound [Cu^{I}(*biq*)$_2$]ClO$_4$ adopt distorted tetrahedral geometries, with similar τ_4 values (0.71 and 0.68 for Cu1 and Cu2, respectively; Table 1 for details). The geometry about each Cu center, while similar to {[Cu^{I}(*biq*)$_2$]ClO$_4$-*biq*} shows that the cations reside in general positions within the lattice. In contrast with compound {[Cu^{I}(*biq*)$_2$]ClO$_4$-*biq*}, the coordinating biquinoline ligands deviate from an orthogonal arrangement with angles formed by the [Cu-N-C-C-N-(Cu)] rings of 84.79(10)° and 82.87(11)° for Cu1 and Cu2, respectively.

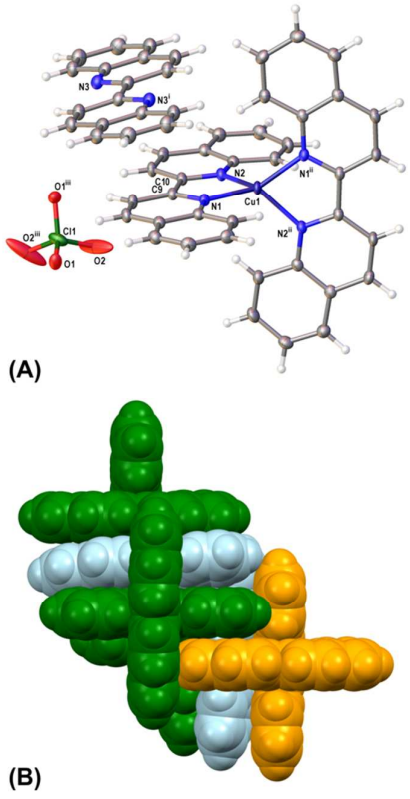

Fig. 1 (A) Crystallographic atom labels for compound {[Cu^{I}(*biq*)$_2$]ClO$_4$-*biq*}; (B) Space-filling packing of compound {[Cu^{I}(*biq*)$_2$]ClO$_4$-*biq*} showing π-stacking interactions; perchlorate anions removed for clarity. Green and yellow: Cu complexes; light blue: uncoordinated biquinoline molecule.

Inspection of the biquinoline ligands reveals a slight twist of the quinoline rings (see Table 2 for periplanar angles). This slight twist induces a small amount of helical nature to the cation that is reflected in the spontaneous resolution of compound [Cu^{I}(*biq*)$_2$]ClO$_4$ (space group P21). As with {[Cu^{I}(*biq*)$_2$]ClO$_4$-*biq*}, π-stacking appears to play a role in the extended packing of these molecules. The terminal phenyl rings of the biquinoline ligands overlap with neighboring phenyl moieties. While the contacts are not as close as {[Cu^{I}(*biq*)$_2$]ClO$_4$-*biq*} above, there is an obvious amount of sterically directed organization of the molecules within the lattice. The water molecules and perchlorate anions occupy interstitial sites. The water molecules are disordered, with only one of the sites having a full occupancy water molecule and the remaining four sites partially occupied water. Although the hydrogen atoms could not be located for these water molecules, they are at reasonable distances from other water molecules and perchlorate oxygen atoms to form hydrogen bonds (Table S2). One perchlorate (Cl1) and the four partial occupancy waters form a chain within the lattice parallel to the crystal-

lographic b-axis, while Cl2 and the fully occupied water molecule form a discrete hydrogen-bonded pair in a pocket with no contacts to the external chain, Figure 2B.

Table 1. Selected bond distances (Å) and angles (°) for compounds {[Cu^{I}(*biq*)$_2$]ClO_4-*biq*} and [Cu^{I}(*biq*)$_2$]ClO_4.

{[Cu^{I}(*biq*)$_2$]ClO_4-*biq*}			
Cu1-N1	1.9847(14)	$N1^{i}$-Cu1-N1	131.02(8)
Cu1-$N1^{i}$	1.9847(14)	$N1^{i}$-Cu1-N2	125.82(6)
Cu1-N2	2.0013(14)	N1-Cu1-N2	81.59(6)
Cu1-$N2^{i}$	2.0013(14)	$N1^{i}$-Cu1-$N2^{i}$	81.59(6)
		N1-Cu1-$N2^{i}$	125.82(6)
		N2-Cu1-$N2^{i}$	116.05(8)
[Cu^{I}(*biq*)$_2$]ClO_4			
Cu1-N4	2.007(3)	N4-Cu1-N2	134.27(14)
Cu1-N2	2.016(4)	N4-Cu1-N3	80.73(12)
Cu1-N3	2.032(3)	N2-Cu1-N3	117.34(14)
Cu1-N1	2.034(4)	N4-Cu1-N1	126.10(14)
		N2-Cu1-N1	80.78(16)
		N3-Cu1-N1	123.44(14)
Cu2-N5	1.973(3)	N5-Cu2-N8	129.52(14)
Cu2-N8	1.988(4)	N5-Cu2-N7	133.98(14)
Cu2-N7	2.004(3)	N8-Cu2-N7	81.44(15)
Cu2-N6	2.012(4)	N5-Cu2-N6	81.21(14)
		N8-Cu2-N6	120.80(14)
		N7-Cu2-N6	114.12(14)

To the best of our knowledge, there is only one other related reported structure {[Cu(*biq*)$_2$]-*biq*} complexes: {[Cu^{I}(*biq*)$_2$]ClO_4-*biq*} above, and Ali's BF_4 salt,[26] both of which crystallize with biquinoline present in the lattice. Two effects on [Cu(*biq*)$_2$]$^+$ complex are caused by non-covalent assembly of the third *biq* in {[Cu^{I}(*biq*)$_2$]ClO_4-*biq*}: one effect in the coordination environment of ion and the other effect on coplanarity of the biquinoline halves relative to complex [Cu^{I}(*biq*)$_2$]ClO_4. As expected, it is these differences that can influence in properties of the complex.

Table 2. Periplanar angles for quinoline moieties within biquinoline ligands and molecules.

Ring 1	Ring 2	Periplanar angle (°)
	{[Cu^{I}(*biq*)$_2$]ClO_4-*biq*}	
N1-C9	$N1^{i}$-$C9^{i}$	3.36(6)
N2-C18	$N2^{ii}$-$C18^{ii}$	0.00(5)
	[Cu^{I}(*biq*)$_2$]ClO_4	
N1-C9	N2-C18	8.86(18)
N3-C27	N4-C36	12.02(16)
N5-C45	N6-C54	2.11(19)
N7-C63	N8-C72	16.64(16)

Symmetry codes: (i) -*x*+3/2, *y*, -*z*+1/2, (ii) -*x*+1, -*y*+1, -*z*+1.

Table 3. Biquinoline intermolecular contacts.[28]

{[Cu^{I}(*biq*)$_2$]ClO_4-*biq*}			
C_g(A)	C_g(B)	C_g(A)…C_g(B) (Å)	C_g(A)…perp(B) (Å)
Cg3	$Cg5^{v}$	3.9084(2)	3.3679
Cg3	$Cg9^{vi}$	3.6619(2)	3.1758
Cg3	$Cg10^{vi}$	3.8274(2)	3.4044
Cg4	$Cg9^{vii}$	3.6368(2)	3.3874
Cg5	$Cg5^{v}$	3.7044(2)	3.3921

C_g(A): Centre of gravity of ring (A/B). C_g(A)…perp(B) is the closest perpendicular contact from ring A to B. C_g3: N1-C1-C6-C7-C8-C9-(N1); C_g4: N2-C10-C11-C12-C13-C18-(N2); C_g5: C1-C2-C3-C4-C5-C6-(C1); C_g9: N3-C19-C24-C25-C26-C27-(N3); C_g10: C19-C20-C21-C22-C23-C24-(C19). Symmetry codes:(v) –*x*+1, -*y*+1, -*z*; (vi): -*x*+1/2, *y*, -*z*+1/2; (vii) *x*+1/2, -*y*+1, *z*+1/2.

[Cu^{I}(*biq*)$_2$]ClO_4			
C_g(A)	C_g(B)	C_g(A)…C_g(B) (Å)	C_g(A)…perp(B) (Å)
C_g4	C_g18^{viii}	3.6051(3)	3.5448
C_g6	C_g18^{ix}	3.6814(3)	3.4594
C_g7	C_g10^{x}	3.7064(3)	3.4915
C_g9	C_g17^{xi}	3.6579(3)	3.5419

C_g4: N2-C10-C11-C12-C13-C18-(N2); C_g6: N4-C28-C29-C30-C31-C36-(N4); C_g7: C1-C2-C3-C4-C5-C6-(C1); C_g9: C19-C20-C21-C22-C23-C24-(C19); C_g10: C31-C32-C33-C34-C35-C36-(C31); C_g17: C37-C38-C39-C40-C41-C42-(C37); C_g18: C49-C50-C51-C52-C53-C54-(C49). Symmetry codes: (viii) *x*-1, *y*, *z*; (ix): -*x*+1, *y*-1/2, *z*+2; (x): -*x*, *y*-1/2, *z*+2; (xi): -*x*+1, *y*-1/2. –*z*+1.

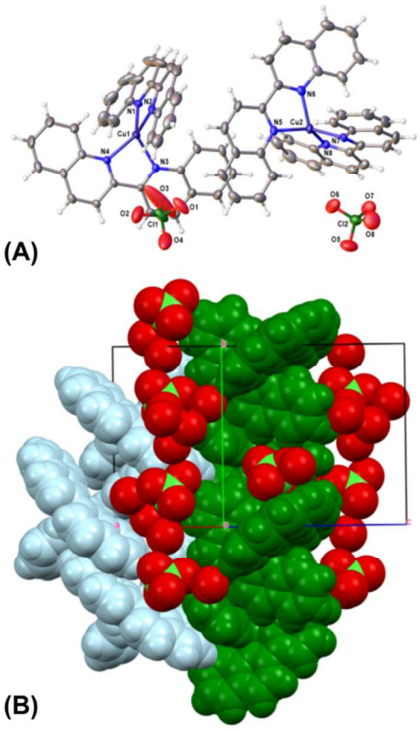

Fig. 2 (A) Crystallographic atom labels for compound [Cu^{I}(*biq*)$_2$]ClO_4; (B) Space-filling packing of compound [Cu^{I}(*biq*)$_2$]ClO_4 showing the hydrogen-bonded channel.

Characterization and stability of solution structures by ^{1}H-NMR spectroscopy: The behaviour of the crystalline samples {[Cu^I(*biq*)$_2$]ClO$_4$-biq} and [Cu^I(*biq*)$_2$]ClO$_4$ was investigated using 1D and 2D ^{1}H-NMR techniques in solution phase of the complexes using $CDCl_3$ and CD_3CN as solvents. The objective was the acquisition of structural information in solution with a view to evaluating their effect on the of UV-Visible spectroscopy and cyclic voltammetry properties. The proton labels were based on those already reported in the literature for the *biq* ligand and confirmed by COSY and NOESY.[29–32] Figure 3 and Fig. S1 provides the numbering of the protons and the ^{1}H chemical shifts (δ/ppm) of the ligands in both complexes. A summary is in the experimental section and table S3. The characteristic proton spectrum of bi-coordinated *biq* was observed for [Cu^I(*biq*)$_2$]ClO$_4$ in $CDCl_3$ showing six aromatic resonances distributed in two doublets [8.95 (H^3) and 8.80 ppm (H^4)] corresponding to the hetero aromatic ring. In addition, a spin system formed for the protons of the fused aromatic ring appears as two doublets 7.95 (H^8) and 7.68 ppm (H^5), and two triplets 7.48 (H^7) and 7.34 ppm (H^6), Fig. 3, spectrum B.

The same pattern of proton signals was observed in CD_3CN where no substitution of the *biq* by solvent took place in an extended time scale (8h) (Fig. S2). In contrast to [Cu^I(*biq*)$_2$]ClO$_4$, the ^{1}H-NMR spectrum of {[Cu^I(*biq*)$_2$]ClO$_4$-*biq*} in $CDCl_3$ exhibits two different signal systems for *biq* in a 2:1 integration ratio, spectrum A in Fig. 3. These assignments were confirmed by 2D COSY spectra, Fig. S3 and S4. The more intense pattern signals is assigned to the [Cu^I(*biq*)$_2$]$^+$ unit in the complex, with signals: 8.93 (H^3; d), 8.90 ppm (H^4; d), for the hetero-ring, and 7.98 (H^8; d), 7.68 (H^5; d), 7.52 (H^7; t) and 7.35 ppm (H^6; t) for the remaining aromatic system. This assignment is in accordance with the high degree of symmetry of the two ligands coordinated to Cu(I) in a manner similar to the spectra of [Cu^I(*biq*)$_2$]ClO$_4$. Relative to this pattern, a second pattern of signals appears at higher fields; this belonging to the uncoordinated *biq* unit in the complex {[Cu^I(*biq*)$_2$]ClO$_4$-*biq*}. It bears a strong resemblance to the proton spectrum of the free *biq*.

On the basis of the strong similarity among the ^{1}H-NMR spectra of {[Cu^I(*biq*)$_2$]ClO$_4$-*biq*} and the corresponding [Cu^I(*biq*)$_2$]$^+$ in [Cu^I(*biq*)$_2$]ClO$_4$ and *biq* spectra (A, B, C in Fig. 3, respectively), it could be concluded that the {[Cu(*biq*)$_2$]ClO$_4$-*biq*} interaction observed in the crystal is lost in solution phase. However, the pattern of signals of coordinated *biq* in {[Cu^I(*biq*)$_2$]ClO$_4$-*biq*} is slightly displaced towards lower fields relative to the same signals in complex [Cu^I(*biq*)$_2$]ClO$_4$. Moreover, the 2D NOESY spectra reveal the correlation between the protons H^3-H$^{3'}$, H^4-H$^{3'}$, H^8-H$^{5'}$, H^6-H$^{7'}$ which is only possible if some type of non-covalent assembly between one unit of [Cu^I(*biq*)$_2$]$^+$ and one *biq* is retained in the solution phase, Fig. 4. These NOESY correlations in {[Cu^I(*biq*)$_2$]ClO$_4$-*biq*} can be attributed to a supramolecular interaction that involves π-π stacking in a similar structure to those observed by X-ray technique, which is sufficiently strong to maintain the association even in a wide range of concentrations of the complex {[Cu^I(*biq*)$_2$]ClO$_4$-*biq*} in $CDCl_3$. These NOESY correlations were observed when low concentrations of *biq* were added to [Cu^I(*biq*)$_2$]ClO$_4$ in accordance with a high association constant (Fig. S5). Thus, small changes have been observed in the chemical shifts of the *biq* signals in highly diluted $CDCl_3$ solution of complex {[Cu^I(*biq*)$_2$]ClO$_4$-*biq*} (around 1.36 x 10^{-5} M), (Fig. 5A). These can be attributed to a dissociative equilibrium of {[Cu^I(*biq*)$_2$]ClO$_4$-*biq*} to yield [Cu^I(*biq*)$_2$]ClO$_4$ and free *biq* , i.e., as is shown in **eq. 1**. This suggests a high stability of the non-covalent assembly of {[Cu^I(*biq*)$_2$]ClO$_4$-*biq*} in $CDCl_3$ solvent; however, the low sensitivity of NMR technique does not permit determination of a reliable equilibrium constant K_D for a dissociative process.

$$\{[\mathrm{Cu}^I(biq)_2]\mathrm{ClO}_4 - biq\} \rightleftarrows [\mathrm{Cu}^I(biq)_2]\mathrm{ClO}_4 + biq \qquad \textbf{eq. 1}$$

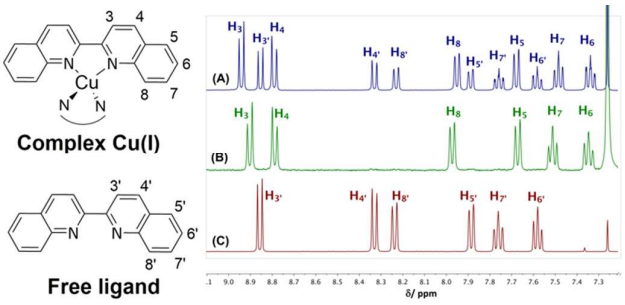

Fig. 3 ^{1}H-NMR spectra of (A) complex {[Cu^I(*biq*)$_2$]ClO$_4$-*biq*} (3.5 x 10^{-3} M), (B) complex [Cu^I(*biq*)$_2$]ClO$_4$ (5.0 x 10^{-5} M) and (C) biquinoline ligand in $CDCl_3$ at 300K.

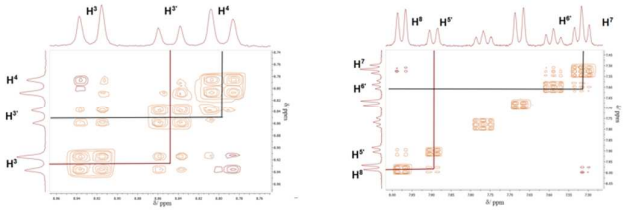

Fig. 4 2D-NOESY interaction spectra of {[Cu^I(*biq*)$_2$]ClO$_4$-*biq*}. All measures in $CDCl_3$ at 300K.

Small changes in resonance frequencies were observed with concentration increases. When Δδ is plotted against {[Cu^I(*biq*)$_2$]ClO$_4$-*biq}* concentration, the behaviour (Fig. 5B) observed suggest the tendency of the complex to form self-assembled species of higher associations.[33,34]

The stability of {[Cu^I(*biq*)$_2$]ClO$_4$-*biq*} also was evaluated in the coordinating solvent, CD_3CN. In contrast to the observations made in $CDCl_3$, the ^{1}H-NMR spectrum of {[Cu^I(*biq*)$_2$]ClO$_4$-*biq*} shows a unique signal pattern, Fig. S6 (spectrum at 298 K). The chemical shifts observed are 8.85 (H^3; d), 8.68 (H^4; d), 8.04 (H^8; d), 7.94 (H^5; d), 7.59 (H^7; t) and 7.54 ppm (H^6).

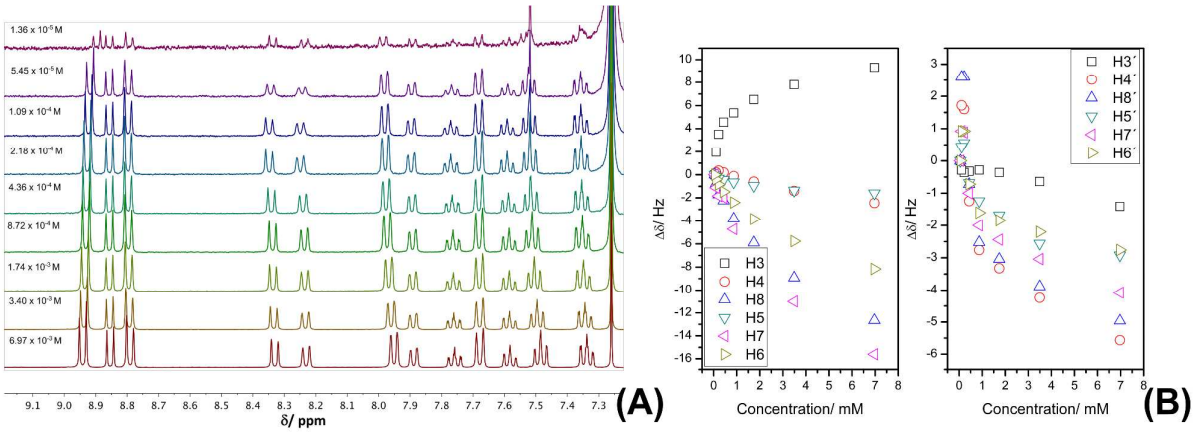

Fig. 5. (A) Concentration-dependence ^{1}H-NMR spectra of complex {[Cu^{I}(*biq*)$_2$]ClO$_4$-*biq*} from 6.97x10^{-3} M to 5.45x10^{-5} M in $CDCl_3$ at 300 K. (B) Concentration versus $\Delta\delta$ for protons of [Cu^{I}(*biq*)$_2$]$^{+}$ unit (left) and biquinoline ligand (right) in complex {[Cu^{I}(*biq*)$_2$]ClO$_4$-*biq*}. $\Delta\delta = \delta i - \delta 0$, where δi correspond to δ observed at any concentration and $\delta 0$ correspond to the lowest concentration measured.

The lineshapes of some protons are very broad (H^4, H^5, H^6) suggesting an intermediate rate for rate for *biq* exchange relative to NMR time scale **(eq. 2).** This observation shows that the three *biq* are chemically equivalent which is evidence for ligand exchange in the complex {[Cu^{I}(*biq*)$_2$]ClO$_4$-*biq*}. At higher temperatures, the spectral definition improves in accordance with a faster exchange rate, Fig. S6.

$$\{[\mathrm{Cu}^{I}(biq)_2]\mathrm{ClO}_4 + biq'\} \rightleftarrows \{[\mathrm{Cu}^{I}(biq)(biq')]\mathrm{ClO}_4 + biq\} \quad \textbf{eq. 2}$$

In conclusion, in $CDCl_3$ solvent dissociation of the stacking interaction in {[Cu^{I}(*biq*)$_2$]ClO$_4$-*biq*} occurs at very low concentrations, in CD_3CN a coordinative exchange between three *biq* exist. This suggests than CD_3CN it participates in this exchange equilibrium by a combination of solvolysis and ligation.[35–41] However, for [Cu^{I}(*biq*)$_2$]ClO$_4$ the ^{1}H-NMR spectrum did not show spectral evidence of *biq* substitution by CD_3CN.

Electrochemical properties: In order to evaluate whether the structural effect caused by non-covalent assembly with the additional *biq* in {[Cu^{I}(*biq*)$_2$]ClO$_4$-*biq*}, which was revealed by X-ray crystallography and 1D/2D NMR techniques in CH_2Cl_2 (*see above*), might influence in the electrochemical and electronic properties, we investigated the electrochemical behaviour of both complexes {[Cu^{I}(*biq*)$_2$]ClO$_4$-*biq*} and [Cu^{I}(*biq*)$_2$]ClO$_4$, in similar solvents to those that were used in the NMR studies.

A summary of the mid-point potential values: $E_{1/2} = (E_{pa}+E_{pc})/2$ vs Ag/AgCl for solutions of {[Cu^{I}(*biq*)$_2$]ClO$_4$-*biq*}, and [Cu^{I}(*biq*)$_2$]ClO$_4$ is presented in Table 4. Cyclic voltammograms of the complexes in dry CH_3CN or CH_2Cl_2 reveal that mass transfer processes are diffusion controlled in both solvents and that redox responses are solvent dependent as was observed in NMR results. The free ligand, *biq* in CH_3CN, undergoes an irreversible, ΔE = 120 mV and $I_{pc}/I_{pa} \neq 1$, single reduction step at $E_{1/2}$ = -1.73 V. No oxidation waves for *biq* were observed within the potential window allowed by the solvent.

Table 4. Summary of cyclic voltammetry data, $E°_{1/2}$ (V) [ΔEp (mV)].

{[Cu^{I}(*biq*)$_2$]ClO$_4$-*biq*}		
Solvent	Metal centered Cu(II)/Cu(I); ΔE/ V	Ligand centered; ΔE/ V
CH_2Cl_2	0.80; 0.079	-1.4
ACN	0.79; 0.081	-1.7
[Cu^{I}(*biq*)$_2$]ClO$_4$		
Solvent	Metal centered Cu(II)/Cu(I)); ΔE/ V	Ligand centered; ΔE/ V
CH_2Cl_2	0.96; 0.099	-1.1; 0.091 -1.4; 0.010
ACN	0.78; 0.072	-1.7; 0.011

*Fc^{+}/Fc= 0.47 V vs Ag/AgCl in CH_3CN
*Fc^{+}/Fc= 0.51 V vs Ag/AgCl in CH_2Cl_2
*$\Delta E = E_{pa}-E_{pc}$

The complex [Cu^{I}(*biq*)$_2$]ClO$_4$, in CH_2Cl_2 shows three quasi reversible redox processes, Fig. 6-C., the Cu(II)/Cu(I) redox process occurs at positive potentials. At negative potential, two redox couples, each via one-electron, were assigned to (biq/biq$^{\bullet -}$) and (biq$^{\bullet -}$/biq^{-2}) processes of the coordinated ligands.[31] On the other hand, in complex {[Cu^{I}(*biq*)$_2$]ClO$_4$-*biq*}, the presence of the non-covalent interaction appears to disrupt this reduction pattern and only one irreversible process is observed, Fig. 6-A.

The Cu(II)/Cu(I) oxidation process for {[Cu^{I}(*biq*)$_2$]ClO$_4$-*biq*}, occurs at less positive potential ($E_{1/2}$ {[Cu^{I}(*biq*)$_2$]ClO$_4$-*biq*} < $E_{1/2}$ [Cu^{I}(*biq*)$_2$]ClO$_4$), this suggests that the presence of π-π stacking in {[Cu^{I}(*biq*)$_2$]ClO$_4$-*biq*}. HOMO destabilization can be explained

by an increment in the distortion from the tetrahedral structure of copper(I) complex,[20,42–44] induced by the presence of π-π stacking between coordinated and non-coordinated *biq* in {[Cu^{I}(*biq*)$_2$]ClO$_4$-*biq*} adduct. Although both complexes shows only small differences in τ4 value (see Crystallographic structure section), is possible to assume that the tetrahedral distortion is increased in solution.[44,45]

The diffusion coefficient value for both complexes was calculated through current (I/ μA) vs square root of scan rate (V$^{1/2}$/ Vs^{-1}) plot for Cu(II)/Cu(I) oxidation process in CH_2Cl_2 (see experimental and Fig. 6-B/D). These values were 5.45 x 10^{-8} cm^2/s for complex {[Cu^{I}(*biq*)$_2$]ClO$_4$-*biq*} and 4,67 x 10^{-7} cm^2/s for complex [Cu^{I}(*biq*)$_2$]ClO$_4$. $D_2 > D_1$, this is indicative that the oxidized complex: {[Cu^{II}(*biq*)$_2$]ClO$_4$-*biq*}, diffuses slower than the oxidized complex [Cu^{II}(*biq*)$_2$]ClO$_4$, can be concluded that the non-covalent interaction is retained in {[Cu^{I}(*biq*)$_2$]ClO$_4$-*biq*}.

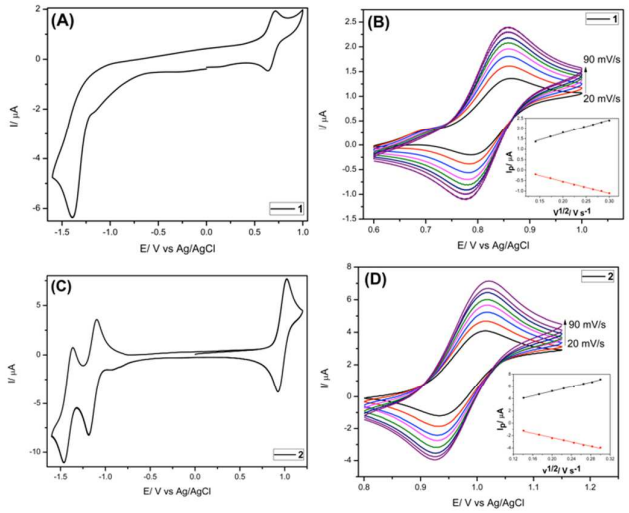

Fig. 6 Cyclic voltammetry of Copper (I) complexes at 50 mV/s (A) {[Cu^{I}(*biq*)$_2$]ClO$_4$-*biq*} and (C) [Cu^{I}(*biq*)$_2$]ClO$_4$. Cu(II)/Cu(I) couple for {[Cu^{I}(*biq*)$_2$]ClO$_4$-*biq*} (B) and [Cu^{I}(*biq*)$_2$]ClO$_4$ (D) at different scan velocity. Insert: i_p vs V$^{1/2}$ in CH_2Cl_2.

On the other hand, when we studied the complexes in a coordinating solvent such as CH_3CN their behaviour is different to that observed in CH_2Cl_2 solvent. The compound [Cu^{I}(*biq*)$_2$]ClO$_4$ in CH_3CN shows multiple redox processes: the same processes described in CH_2Cl_2 and one reduction process and one anodic stripping peak (Fig. S9). An adequate interpretation of this behaviour is difficult, however, as the results suggest that in coordinating solvent such as CH_3CN, an equilibrium with the heteroleptic intermediary [Cu(*biq*)$(CH_3CN)_2]^+$ can be generated in low concentration as follows (**eq 3**).

$$[\mathrm{Cu}^{I}(biq)_2]\mathrm{ClO}_4 + 2\mathrm{CH}_3\mathrm{CN} \rightleftarrows [\mathrm{Cu}^{I}(biq)(\mathrm{CH}_3\mathrm{CN})_2]\mathrm{ClO}_4 + biq \qquad \textbf{eq.3}$$

From the equilibrium described above (**eq. 3**), the reduced complex [Cu^{I}(*biq*)(biq$^{\bullet-}$)]^0 can undertake a charge rearrangement (and for resulting in the presence of the anodic stripping peak). The behaviour is presented in **eq. 4-5**. The same effect would be obtained from intermediary complex (**eq. 4**). The IR-SEC experiments showed vibrational changes at (ν/ cm^{-1}~1600), probably assigned to C=C or N=N, suggesting the formation of the [Cu^{I}(*biq*)$(CH_3CN)_2]^+$ specie (Fig. S10).

$$[\mathrm{Cu}^{I}(biq)_2]^+ + \mathrm{ClO}_4^- + 1e^- \rightleftarrows [\mathrm{Cu}^{I}(biq)(biq^{\bullet-})]^0 + \mathrm{ClO}_4^- \qquad \textbf{eq. 4}$$

$$[\mathrm{Cu}^{I}(biq)(biq^{\bullet-})]^0 + \mathrm{ClO}_4^- \rightleftarrows \mathrm{Cu}^0 + 2biq + \mathrm{ClO}_4^- \qquad \textbf{eq. 5}$$

On the other hand, {[Cu^{I}(*biq*)$_2$]ClO$_4$-*biq*} in CH_3CN is different to **eq. 2** and **eq. 4** proposed previously for [Cu^{I}(*biq*)$_2$]ClO$_4$. The additional *biq* appears to disrupt these precesses. Compound {[Cu^{I}(*biq*)$_2$]ClO$_4$-*biq*} in CH_3CN shows only two irreversible reduction processes at E_{pa}=-1.28 V and E_{pa}=-1.73 V. In the same way, the Cu(II)/Cu(I) process values in CH_3CN, $E_{1/2}$ = 0.79 V for {[Cu^{I}(*biq*)$_2$]ClO$_4$-*biq*} and 0.78 V for [Cu^{I}(*biq*)$_2$]ClO$_4$ are similar in accordance to equation 2.

As shown above, both complexes are solvent dependent. In non-coordinating solvent it is possible to obtain evidence for the existence of the adduct {[Cu^{I}(*biq*)$_2$]ClO$_4$-*biq*} even in a high ionic strength environment (0.1M TBAClO$_4$) as used in cyclic voltammetry measurements.

UV-Vis spectroscopy: Considering that both complexes have different NMR structural and electrochemical behaviour in solution and show solvent dependence, we have carried out a UV-Vis study in similar conditions to those used in cyclic voltammetry studies (CH_2Cl_2 and TBAClO$_4$) in order to evaluate both the stacking assembly effect and the impact of supporting electrolyte on electronic properties of {[Cu^{I}(*biq*)$_2$]ClO$_4$-*biq*}. A very broad MLCT band with a similar spectral profile is observed for both complexes in solution in both the CH_2Cl_2 and CH_3CN solvents with λ_{max} values close to 550nm (Fig. 7 and Fig. S11 and S12). Thus, no discernible differences between the spectra are observed. The molar extinction coefficients values (**ε**) for [Cu^{I}(*biq*)$_2$]ClO$_4$ in both solvents used are relatively similar to each other (Table S4). The ε values of {[Cu^{I}(*biq*)$_2$]ClO$_4$-*biq*} are slightly greater than the value exhibited by [Cu^{I}(*biq*)$_2$]ClO$_4$ but cannot be determined accurately. On the other hand, a good linear regression (R^2> 0.99) was obtained from absorbance vs concentration plots in all cases (Fig. 7). Although this might suggest the presence of only one specie absorbing in each case, the similarity in ε values and the presence of ion pairing effects do not discount contributions of species in lower concentrations as the proposed in **eq. 1** and **eq. 3** from both NMR and electrochemical discussion.

However, these data suggest that {[Cu^{I}(*biq*)$_2$]ClO$_4$-*biq*} is mainly retained as non-covalent assembly between one complex unit and one *biq* in non-coordinative solvents, i.e. in CH_2Cl_2 and $CHCl_3$. However, this is not necessarily obvious in the high ionic strength as used in the cyclic voltammetry. With a focus on clarifying this last point, a plot of absorbance at 549 vs an increasing amount of *biq* added to [Cu^{I}(*biq*)$_2$]ClO$_4$ solution in CH_2Cl_2, in presence of supporting electrolyte was carried out

(Fig. 8 and S13 respectively). An initial increase in absorbance is observed at low added [*biq*] reaching a maximum when the $[Cu^{I}(biq)_2]ClO_4$/*biq* ratio is close to 1:1 (Figure 8B). This provides further evidence of the tendency toward formation of non-covalent adducts predominating in concentration even in high ionic strength.

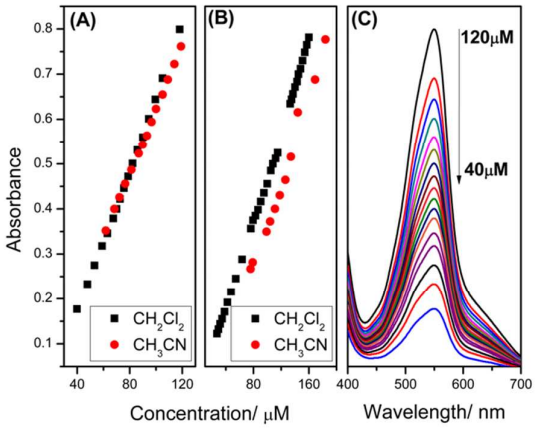

Fig. 7 Plot of the absorbance vs concentration for similar range of concentrations in CH_2Cl_2 (black line) and CH_3CN (red line) for (A) $\{[Cu^{I}(biq)_2]ClO_4$-*biq*$\}$ and (B) $[Cu^{I}(biq)_2]ClO_4$. (C) UV-Vis spectra of $\{[Cu^{I}(biq)_2]ClO_4$-*biq*$\}$ in CH_2Cl_2 solutions at different concentrations (120 μM to 40 μM).

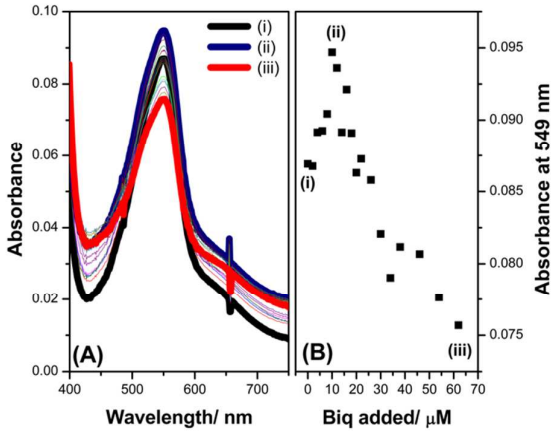

Fig. 8 (A) UV-Vis spectra of MLCT recorded with solutions of $[Cu^{I}(biq)_2]ClO_4$ of 1 x 10^{-5} M in presence of several *biq* concentrations in CH_2Cl_2 solvent with 0.1 M $TBAClO_4$; (B) Plot of the absorbance at 549 nm (MLCT band) vs *biq* concentration. (i) Correspond to initial point, $[Cu^{I}(biq)_2]ClO_4$ only; (ii) Correspond to 1:1 relation between $[Cu^{I}(biq)_2]ClO_4$ and *biq*; (iii) Correspond to final point, *biq* excess.

At higher [*biq*], above the 1:1 molar ratio, the absorption of the MLCT decreases. This is attributed to species of greater association between $\{[Cu^{I}(biq)_2]ClO_4$-*biq*$\}$ and *biq*, for example $\{[Cu^{I}(biq)_2]ClO_4$-$(biq)_n\}$. A tendency toward higher order associations of this complex was observed in NMR studies in $CDCl_3$ (see before). To attempt to clarify this behavior, we titrated a solution of $[Cu^{I}(biq)_2]ClO_4$, 1x10^{-5} M (A solution) with a mixture of $\{[Cu^{I}(biq)_2]ClO_4$-*biq*$\}$, 1x10^{-5} M and *biq* 1x10^{-4} M (B solution). This system always provides an excess of *biq* in the titrated solution. The plot of absorbance vs B solution concentration shows that the absorbance at 550 decreases in the same way as in the previously experiment, (Fig. S14).

Experimental

Materials

2,2'-biquinoline (*biq*) from Sigma-Aldrich was used as received. Acetonitrile (CH_3CN), dichloromethane (CH_2Cl_2) and chloroform ($CHCl_3$) and deuterated solvents were obtained from Merck and used as received. CH_3CN and CH_2Cl_2 were specially treated for use in electrochemistry studies.

$\{[Cu^{I}(biq)_2]ClO_4$-*biq*$\}$ syntheses

The precursor of the complexes, $[Cu^{I}(CH_3CN)_4]ClO_4$, was prepared according to literature reports.[46] Complex $[Cu(biq)_2]ClO_4$ was prepared following a literature protocol.[19] Two types of crystals were obtained from a concentrated solution of $[Cu(biq)_2]ClO_4$ in 1:1 (v:v) CH_2Cl_2/CH_3CN when the solvent was slowly evaporated. Small amounts of compound $\{[Cu(biq)_2]ClO_4$-*biq*$\}$ appeared as red colored crystals while compound $[Cu(biq)_2]ClO_4$ formed as purple colored crystals. To obtain pure $\{[Cu(biq)_2]ClO_4$-*biq*$\}$, *biq* was added to a concentrated solution of $[Cu(biq)_2]ClO_4$ in equivalent quantities (Fig. S15).

Complex **$\{[Cu^{I}(biq)_2]ClO_4$-*biq*$\}$**, *Elemental analyses:* Found: C=68.33, H= 4.23, N=8.69, Calc. for $C_{54}H_{36}ClCuN_6O_4{\cdot}H_2O$: C= 68.28, H= 4.03, N= 8.85%. Yield: 70%. ^{1}H-NMR δ($CDCl_3$, 300K)/ppm: 8.93 (H^3; 4H; d; J_{3-4}=8.86 Hz), 8.90 (H^4; 4H; d), 7.98 (H^8; 4H; d; J_{8-7}=7.71 Hz), 7.68 (H^5; 4H; d; J_{5-6}=7.52Hz), 7.52 (H^7; 4H; t; J_{7-6}=7.41 Hz), 7.35 (H^6; 4H; t), 8.85 ($H^{3'}$; 2H; d; $J_{3'-4'}$=8.70 Hz), 8.34 ($H^{4'}$; 2H; d), 8.24 ($H^{8'}$; 2H; d; $J_{8'-7'}$=8.02 Hz), 7.90 ($H^{5'}$; 2H; d; $J_{5'-6'}$=7.72 Hz), 7.77 ($H^{7'}$; 2H; t; $J_{7'-6'}$=7.66 Hz), 7.59 ($H^{6'}$; 2H; t). UV-Vis: $\lambda_{max}(CH_2Cl_2)$/nm (ε/dm^3 mol^{-1} cm^{-1}): 549.0 (5900), 206.5, 225, 258, 337.5, 325, 313, 300(s).

Complex **$[Cu(biq)_2]ClO_4$**, *Elemental analyses:* Found: C=60.55, H= 3.78, N=7.86, Calc. for $C_{36}H_{24}ClCuN_4O_4{\cdot}(H_2O)_2$: C=60.76, H=3.97, N=7.87. Yield: 89.67%. ^{1}H-NMR δ($CDCl_3$, 300K)/ppm: 8.95 (H^3; 4H; d; J_{3-4}=8.87 Hz), 8.80 (H^4; 4H; d), 7.95 (H^8; 4H; d; J_{8-7}=7.66 Hz), 7.68 (H^5; 4H; d; J_{5-6}=7.47 Hz), 7.48 (H^7; 4H; t; J_{7-6}=7.39 Hz), 7.34 (H^6; 4H; t). UV-Vis: $\lambda_{max}(CH_2Cl_2)$/nm (ε/dm^3 mol^{-1} cm^{-1}): 549.0 (4925), 207.5, 259, 285(s), 298.25, 313.5, 326.5, 338.5, 357.

IR more characteristics frequencies [KBr, (ν/cm^{-1})]: 610 and 1095 (ClO_4, strong), 1504 (C=N stretching, medium), 1591 (C=C stretching, medium) for complex $\{[Cu^{I}(biq)_2]ClO_4$-*biq*$\}$ and $[Cu(biq)_2]ClO_4$ (Fig. S16). Mass analysis (m/z)= 575.0 for $[Cu(biq)_2]^+$ in both compounds ($\{[Cu^{I}(biq)_2]ClO_4$-*biq*$\}$ and $[Cu(biq)_2]ClO_4$) because a very dilute solution is necessary for this kind of experiment (Fig. S17).

Materials and methods

NMR spectrometer: ^{1}H-NMR, ^{1}H-^{1}H 2D-COSY, ^{1}H-^{1}H 2D-NOESY spectra were recorded in a Bruker Avance 400 MHz spectrometer (400.133 MHz for ^{1}H) equipped with a 5 mm multinuclear broad-band dual probe head, incorporating a **z**-gradient coil. The measurements were carried out in $CDCl_3$ and CD_3CN at 300 K. ^{1}H-NMR-VT experiments were carried out in CD_3CN at temperatures between 243-345 K. Chemical shifts (δ/ppm) were calibrated with respect to the solvent signal (δ=7.26, $CDCl_3$ and 1.94, CD_3CN) and reported relative to TMS. *UV-Visible spectroscopy:* The UV-Visible spectra were obtained on a Shimadzu Multispec 1501 spectrophotometer using quartz cells of 1.00 cm of path length in CH_2Cl_2 and ACN solvents with a complex concentration of 1.00 x 10^{-4} M. *Elemental analyses*: MIDWEST MICROLAB, Indianapolis, United States. *Electrochemistry:* All measurements were carried out using a Basi Epsilon potentiostat (Bioanalytical Systems Inc.). The electrochemical cell used consists of a glass chamber, provided with platinum disk electrode as working electrode, Ag/AgCl as reference electrode, adequate for organic solvents, and a platinum wire as auxiliary electrode. The supporting electrolyte tetrabutylammonium perchlorate, (TBA)ClO_4, was dried for 24 h. under vaccum before it was incorporated in the solutions. The working electrode was cleaned with polishing diamond 1.0 μM and polishing alumina 0.1 μM and then rinsed with water and methanol. The cyclic voltammetry measurements were performed at room temperature under N_2, using solutions containing concentrations 1 mM of the complexes and 0.1M (TBA)ClO_4 in either dry ACN or CH_2Cl_2.[47–49] The electroactive area of the working electrode was calculated from the absorption of hydrogen in the platinum electrode when immersed in 0.5 M H_2SO_4.[50] The calculated experimental area was 0.10 cm^2 and the geometric area is 0.126 cm^2. The diffusion coefficients of the complexes were calculated with the *Randles-Sevcik* equation[51]: $\mathrm{Ip} = (2.69\mathrm{x}10^5)\mathrm{n}^{3/2}\mathrm{AD}^{1/2}\mathrm{cV}^{1/2}$ where: I_p = current for the process, n= number of electrons transferred, A = electrode electroactive area, D = diffusion coefficient, c = concentration of compound, V= scan velocity. *X-Ray crystallography*: Arbitrary spheres of data were collected on a red block-like crystal for (**1**) and orange plate-like crystal for (**2**), having respective dimensions of 0.238 × 0.142 × 0.110 mm (**1**) and 0.496 × 0.236 × 0.215 mm (**2**), on a Bruker Kappa X8-APEX-II diffractometer using a combination of ω- and ϕ-scans of 0.5°.[52] Data were corrected for absorption and polarization effects and analysed for space group determination. The structure was solved by intrinsic phasing methods and expanded routinely.[53] The model was refined by full-matrix least-squares analysis of F^2 against all reflections.[54] All non-hydrogen atoms were refined with anisotropic atomic displacement parameters. Unless otherwise noted, hydrogen atoms were included in calculated positions. Atomic displacement parameters for the hydrogens were tied to the equivalent isotropic displacement parameter of the atom to which they are bonded (U_{iso}(H) = 1.5U_{eq}(C) for methyl, 1.2U_{eq}(C) for all others). A summary for both crystals data is presented in table S1.

Conclusions

Two complexes of Cu(I) were obtained by using two stoichiometric Cu(I):*biq* ratios, 1:2 and 1:3, in their synthesis. The first, $[Cu^I(biq)_2]ClO_4$, corresponds to a classic homoleptic complex while the second, {$[Cu^I(biq)_2]ClO_4$-*biq*}, is a supramolecular compound. The stability of the supramolecular assembly is provided by a π-π stacking interaction of an uncoordinated *biq* with a coordinated *biq* ligand. Solution behaviour of both complexes is strongly solvent dependent. In the coordinating solvent CH_3CN, dissociation of a *biq* ligand is observed and rapid ligand exchange is noted by NMR and coherently, not influence the HOMO energy. In non-coordinating solvents such as CH_3Cl and CH_2Cl_2, there is evidence for a π-stacking interaction similar to the one found in the solid state. This supramolecular assembly in {$[Cu^I(biq)_2]ClO_4$-*biq*}, induces conformational rearrangement around metal centre destabilizes the HOMO relative to the homoleptic complex. Such non-covalent interactions open newly expectations to the design of Cu (I) compounds with unusual and improved properties.

Conflicts of interest

There are no conflicts to declare

Acknowledgements

The authors acknowledgment to “PMI PUC 1203: Convenio de Desempeño de Internacionalización de Doctorado”, Project RC 130006, CILIS, granted by Fondo de Innovación para la Competitividad, del Ministerio de Economía, Fomento y Turismo, Chile. FONDECYT 1181226, FONDECYT 1140193, CONICYT Doctoral Fellowships 21140356. FONDEQUIP-EQM 150106. FONDEQUIP-EQM 130032. Luksburg Foundation Collaboration Grants program for support. Part of this work was also carried out in the Notre Dame Radiation Laboratory (NDRL). The NDRL is supported by the Division of Chemical Sciences, Geosciences and Biosciences, Basic Energy Sciences, Office of Science, United States Department of Energy through grant number DE-FC02-04ER15533. This is contribution number NDRL 5215. The authors acknowledge Diego Alonzo Quezada (Laboratorio de electroquímica y fisicoquímica de sólidos, Facultad de Química y Biología, Universidad de Santiago de Chile – *diego.quezada.s@usach.cl*) for FT-IR spectroelectrochemistry measurements of the complex.

Notes and references

CCDC 1588824-1588825 contains the supplementary crystallographic data for this paper. These data can be obtained free of charge from The Cambridge Crystallographic Data Centre via www.ccdc.cam.ac.uk/structures.

1 A. Pastor and E. Martínez-Viviente, *Coord. Chem. Rev.*, 2008, **252**, 2314–2345.
2 A. Joosten, Y. Trolez, J.-P. Collin, V. Heitz and J.-P. Sauvage, *J. Am. Chem. Soc.*, 2012, **134**, 1802–1809.
3 L. Lemus, J. Guerrero, J. Costamagna, R. Lorca, D. H. Jara, G. Ferraudi, A. Oliver and A. G. Lappin, *Dalton. Trans.*, 2013, **42**, 11426–11435.
4 C. Piguet, M. Borkovec, J. Hamacek and K. Zeckert, *Coord. Chem. Rev.*, 2005, **249**, 705–726.
5 A. Lützen, *Angew. Chemie - Int. Ed.*, 2005, **44**, 1000–1002.
6 R. S. Forgan, J.-P. Sauvage and J. F. Stoddart, *Chem. Rev.*, 2011, **111**, 5434–5464.
7 C. O. Ditrich-Buchecker, J.-F. Nierengarten and J.-P. Sauvage, *Tetrahedron Lett.*, 1992, **33**, 3625–3628.
8 R. F. Carina, C. Dietrich-Buchecker and J.-P. Sauvage, *J. Am. Chem. Soc.*, 1996, **118**, 9110–9116.
9 G. Rapenne, C. Dietrich-Buchecker and J. P. Sauvage, *J. Am. Chem. Soc.*, 1996, **118**, 10932–10933.
10 D. J. Cárdenas and J.-P. Sauvage, *Inorg. Chem.*, 1997, **36**, 2777–2783.
11 T. Jørgensen, J. Becher, J. C. Chambron and J. P. Sauvage, *Tetrahedron Lett.*, 1994, **35**, 4339–4342.
12 M. Meyer, A. M. Albrecht-Gary, C. O. Dietrich-Buchecker and J. P. Sauvage, *J. Am. Chem. Soc.*, 1997, **119**, 4599–4607.
13 D. J. Cárdenas, A. Livoreil and J. P. Sauvage, *J. Am. Chem. Soc.*, 1996, **118**, 11980–11981.
14 J.-M. Lehn, *Supramolecular chemistry*, Vch, Weinheim, 1995, vol. 1.
15 M. Albrecht, *Chem. Rev.*, 2001, **101**, 3457–3498.
16 J. M. Lehn, A. Rigault, J. Siegel, J. Harrowfield, B. Chevrier and D. Moras, *Proc. Natl. Acad. Sci.* , 1987, **84**, 2565–2569.
17 C. L. Linfoot, P. Richardson, T. E. Hewat, O. Moudam, M. M. Forde, A. Collins, F. White and N. Robertson, *Dalton. Trans.*, 2010, **39**, 8945.
18 K. A. Wills, H. J. Mandujano-Ramírez, G. Merino, D. Mattia, T. Hewat, N. Robertson, G. Oskam, M. D. Jones, S. E. Lewis and P. J. Cameron, *RSC Adv.*, 2013, **3**, 23361–23369.
19 Y. Jahng, J. Hazelrigg, D. Kimball, E. Riesgo, F. Wu and R. P. Thummel, *Inorg. Chem.*, 1997, **36**, 5390–5395.
20 E. C. Riesgo, Y.-Z. Hu, F. Bouvier, R. P. Thummel, D. V Scaltrito and G. J. Meyer, *Inorg. Chem.*, 2001, **40**, 3413–3422.
21 Thomas. C. W. Mak, Xiu Chun Wang, and Henry N.C. Wong, *Tetrahedron Lett.*, 1987, **28**, 5833–5836.
22 J. Vallejos, I. Brito, A. Cárdenas, M. Bolte, S. Conejeros, P. Alemany and J. Llanos, *Polymers (Basel).*, 2016, **8**, 46.
23 P. O. Oguadinma, A. Rodrigue-Witchel, C. Reber and F. Schaper, *Dalton. Trans.*, 2010, **39**, 8759.
24 G. R. Cayley and D. W. Margerum, *J. Chem. Soc. Chem. Commun.*, 1974, 1002–1004.
25 D. H. Jara, L. Lemus, L. Farías, E. Freire, R. Baggio and J. Guerrero, *Eur. J. Inorg. Chem.,* 2012, 1579–1583.
26 B. F. Ali, K. Al-Sou'od, N. Al-Ja'ar, A. Nassar, M. H. Zaghal, Z. Judeh, R. Al-Far, M. Al-Refai, M. Ibrahim, K. Mansi and K. H. Al-Obaidi, *J. Coord. Chem.*, 2006, **59**, 229–241.
27 L. Yang, D. R. Powell and R. P. Houser, *Dalton Trans.*, 2007, 955–964.
28 A. L. Spek, *Acta Crystallogr. Sect. D Biol. Crystallogr.*, 2009, **65**, 148–155.
29 S. A. Moya, J. Guerrero, R. Pastene, R. Schmidt, R. Sariego, R. Sartori, J. Sanz-Aparicio, I. Fonseca and M. Martínez-Ripoll, *Inorg. Chem.*, 1994, **33**, 2341–2346.
30 R. P. Thummel and F. Lefoulon, *Inorg. Chem.*, 1987, **26**, 675–680.
31 J. Guerrero, L. Farías, L. Lemus, A. Quintanilla, A. Mena, L. Cortez, R. F. Baggio and M. T. Garland, *Polyhedron*, 2006, **25**, 9–16.
32 S. A. Moya, J. Guerrero, F. J. Rodriguez-Nieto, E. Wolcan, M. R. Féliz, R. F. Baggio and M. T. Garland, *Helv. Chim. Acta*, 2005, **88**, 2842–2860.
33 L. Fielding, *Tetrahedron*, 2000, **56**, 6151–6170.
34 R. B. Martin, *Chem. Rev.*, 1996, **96**, 3043–3064.
35 S. Bait and J. Meuldijk, 1979, 843–849.
36 C. F. Weber and R. Van Eldik, *Eur. J. Inorg. Chem.*, 2005, 4755–4761.
37 J. P. Kuczynski, B. H. Milosavljevic, A. G. Lappin and J. K. Thomas, *Chem. Phys. Lett.*, 1984, **104**, 149–152.
38 R. G. Wilkins, *Kinetics and Mechanism of Reactions of Transition Metal Complexes*, 2nd Edition.
39 U. M. Frei and G. Geier, *Inorg. Chem.*, 1992, **31**, 187–190.
40 J. H. Cameron, A. Graham, J. M. Winfield and A. Mcauley, *J. Chem. Soc., Dalton. Trans.*, **1981**, 0, 2172–2175.
41 L. Lemus, J. Guerrero, J. Costamagna, G. Estiu, G. Ferraudi, A. G. Lappin, A. Oliver and B. C. Noll, *Inorg. Chem.*, 2010, **49**, 4023–4035.
42 J. Guerrero, L. Cortez, L. Lemus, L. Farías, J. Costamagna, C. Pettinari, M. Rossi and F. Caruso, *Inorganica Chim. Acta*, 2010, **363**, 3809–3816.
43 M. K. Eggleston, D. R. McMillin, K. S. Koenig and A. J. Pallenberg, *Inorg. Chem.*, 1997, **36**, 172–176.
44 M. T. Miller, P. K. Gantzel, T. B. Karpishin and L. Jolla, *Inorg. Chem.*, 1999, **38**, 3414–3422.
45 L. X. Chen, G. B. Shaw, I. Novozhilova, T. Liu, G. Jennings, K. Attenkofer, G. J. Meyer and P. Coppens, *J. Am. Chem. Soc.*, 2003, **125**, 7022–7034.
46 A. L. Kubas, G. J., Monzyk, B. and Crumbliss, *Tetrakis(Acetonitrile)Copper(I) Hexafluorophosphate*, John Wiley & Sons, Inc., Hoboken, NJ, USA, 1979.
47 W. L. F. Armarego, ed. W. L. F. B. T.-P. of L. C. (Eighth E. Armarego, Butterworth-Heinemann, 2017, pp. 1–70.
48 W. L. F. Armarego, ed. W. L. F. B. T.-P. of L. C. (Eighth E. Armarego, Butterworth-Heinemann, 2017, pp. 95–634.
49 W. L. F. Armarego, ed. W. L. F. B. T.-P. of L. C. (Eighth E. Armarego, Butterworth-Heinemann, 2017, pp. 71–94.
50 J. M. Doña Rodríguez, J. A. Herrera Melián and J. Pérez Peña, *J. Chem. Educ.*, 2000, **77**, 1195.
51 A. J. Bard, L. R. Faulkner, J. Leddy and C. G. Zoski, *Electrochemical methods: fundamentals and applications*, Wiley New York, 1980, vol. 2.
52 Bruker AXS. (2014). APEX-2. Bruker-Nonius AXS, Madison, Wisconsin, USA.
53 G. M. Sheldrick, *Acta Crystallogr. Sect. A Found. Crystallogr.*, 2015, **71**, 3–8.

54 G. M. Sheldrick, *Acta Crystallogr. Sect. C Struct. Chem.*, 2015, **71**, 3–8.

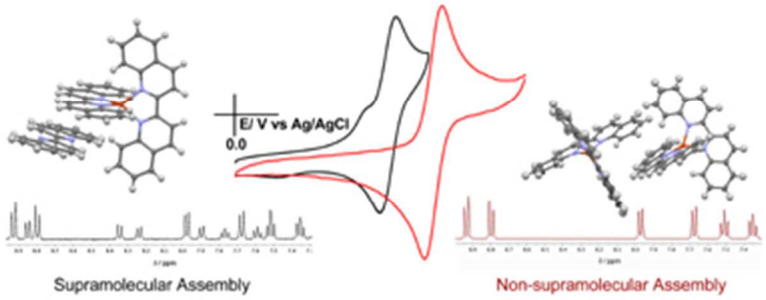
E/ V vs Ag/AgCl
0.0
Supramolecular Assembly
Non-supramolecular Assembly